Towards Wideband Hyperthermia Treatment System

N. Nizam-Uddin, Wazie Alkadri, Waqar Ahmad Malik, Ibrahim Elshafiey, and Abdel Fattah Sheta

Department of Electrical Engineering
King Saud University, Riyadh, Kingdom of Saudi Arabia
{enizamuddin, walkadri, wmalik, ishafiey, asheta}@ksu.edu.sa

Abstract ─ This paper presents an overview of design and functionality of the essential modules proposed to build a wideband hyperthermia system. Description is provided of the waveform shaper, power amplifier and applicator array modules. Big data analysis is presented to accelerate energy localization depending on a time reversal technique. Simulation results are provided assuming a cylindrical head phantom characterized with wideband dispersive tissue properties, and the obtained field maps are shown in different planes to visualize energy localization process. Results reveal that wideband operation has the potential to enhance energy localization in deep tumor regions while eradicating hot spots, as compared to conventional narrowband systems.

Index Terms ─ Big data, double-ridge horn antenna, hyperthermia treatment, time reversal focusing, wideband power amplifier.

I. INTRODUCTION

Hyperthermia is known to be a promising therapeutic modality for curing cancer. In electromagnetic (EM) hyperthermia systems, the induced EM energy is used to elevate the temperature of malignant tissues to 40-45C° [1, 2]. Used in adjunct with radiotherapy and chemotherapy, hyperthermia treatment can reduce the vitality of malignant tissues and increase the effectiveness of therapeutic plans [3, 4]. Energy localization is required to be achieved onto intended regions without affecting the surrounding healthy tissues [5]. An effective hyperthermia treatment planning that caters for variations in age, size, tumor location and tissue properties is challenging. Development of a patient-specific treatment plan can be achieved, depending on robust energy focusing techniques along with high flexibility in system technical parameters. This research aims at enhancing the degrees of freedom of hyperthermia treatment system by using various channels and adopting wideband operation. Elevating the number of degrees of freedom allows the optimization of system performance on the expense of augmenting the complexity of data processing and analysis. Progress in big data analysis however, can be used to alleviate the complexity of developing patient-specific hyperthermia treatment systems.

With exponential growth of associated data in health care domains, big data is gaining considerable attention in terms of reducing cost, enhancing performance, developing standards and improving patient care [6, 7]. Characterizing data by volume, veracity, variety and velocity, big data analysis accelerates innovations in health care units [8, 9]. The evaluation tools associated with big data allow shifting from population based to patient specific plans. Patient specific planning allows improving the efficacy and specificity of treatment, and enhances patient care and comfort.

This research proposes a modular treatment system that can be used for patient specific treatment of brain tumors. The main modules include head model, applicator array, power amplifier PA array, and waveform shaper. The modular nature of the proposed system provides flexibility of system parameters to allow optimizing energy localization to required regions, while reducing associated hot spots in healthy tissues.

From big data perspective, the *volume* represents the complexity of our system related to the parameters of various modules. This includes the patient head model that identifies the size and location of each tumor as well as the wideband dispersive model of brain tissues. Data volume is also related to the characteristics of antenna element of the applicator array linked with system channels. Each channel is also associated with a PA that is characterized by frequency band of operation, maximum power, linearity and efficiency. In order to ensure the *veracity* of the proposed system we characterize each module under wideband operation. The waveform-shaping module is concerned with data *variety*. This module is associated with identifying the number of enabled channels as well as designing the excitation signal for each channel. The optimization tool associated with waveform-shaping module controls the *velocity* of the system, and we devise a robust wideband time reversal optimization tool to meet the velocity

requirements of the proposed system.

II. PROTOTYPE OF WIDEBAND HYPERTHERMIA SYSTEM

The proposed multi-channel wideband hyperthermia system for enhanced energy localization is shown in Fig. 1. The waveform-shaping module depends upon an optimization tool to obtain digital form of the excitation signal of each channel. The optimization tool estimates the optimum values of the phase and magnitude of each frequency subcarrier to achieve constructive interference or EM energy at the tumor region and destructive interference elsewhere.

The optimization tool depends on accurate patient specific head model to account for the wideband dispersive properties of various tissues. A linearization tool is also integrated with the waveform-shaping module in order to equalize the distortion introduced by the power amplifier under wideband excitation, which can diminish the process of energy localization.

Each channel consists of a digital to analog converter (DAC), and high power wideband amplifier to provide enough power to maintain required temperature levels at tissues. The wideband applicator elements should maintain appropriate radiation in the frequency band of operation. A feedback mechanism is added to monitor temperature maps and control the waveform-shaping module. Description of our proposed system is described next.
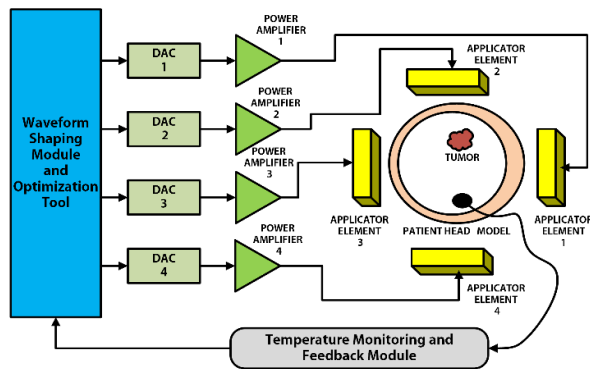

Fig. 1. Prototype of four-channel wideband hyperthermia treatment system.

III. MODULAR DESCRIPTION OF THE PROPOSED SYSTEM

Based on Fig. 1, we present an overview of the design and functionality of each module independently with a focus on the response of each module under wideband excitation.

A. The head model module

Patient-specific model and properties of head tissue can be utilized to optimize system performance. In this research, the analysis depends on heterogeneous head phantom represented by a four-layered cylinder of radius 10 cm is developed in CST Microwave Studio [10]. The inner four layers depicts brain tissue (radius = 8cm), gray matter (radius = 8.4cm), cerebrospinal fluid (CSF) (radius = 8.9cm) and skull (radius = 9.4cm) respectively. This model is shown in Fig. 2.
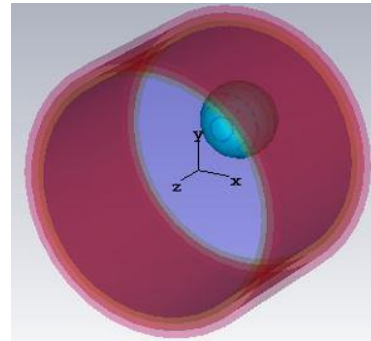

Fig. 2. Illustration of head phantom with an embedded tumor.

The tumor is taken to be of spherical shape (radius is 2.5 cm), and is located at x = 3 cm, y = 4 cm and z = 0, where the origin is set at the center of the phantom. The dispersive dielectric properties of brain tissue and tumor under wideband excitation are chosen in accordance with [11-13].

B. The applicator module

Several designs have been considered as heating applicators for hyperthermia treatment over the past few years. It includes Vivaldi [14], antipodal [15], microstrip [16, 17] and horn [18] antennas. Double ridge horn antenna can be designed to provide good performance in a very large bandwidth. Therefore, the traditional horn antenna has been replaced by double ridge horn antennas (DRHA) because of high gain, good directivity performance, low back radiation, low voltage standing wave ratio, and high peak power handling capability in wide bandwidth, which makes it a promising heating source for hyperthermia treatment [19, 20]. Recent developments in DRHA design are reported in [21, 22].

Here in this research we propose a double ridge horn antenna comprising of coaxial feeding, waveguide part, and two side ridges made of base ridges and flares as shown in Fig. 3.

The exponential section of the ridge profile is approximated by the following exponential equation:
$$f(x) = 0.02x + 2.5e^{0.0305x}. \qquad (1)$$
Where x is the axial length in millimeter along the horn from the straight section of the ridge, and f(x) is the perpendicular distance in millimeter from the centerline of the horn. The physical dimensions of the proposed DRHA are aperture width = 100 mm, aperture height =

100 mm and antenna length = 111 mm. We choose a minimum distance of 5 mm between proposed antenna and head phantom illustrated in Fig. 4 for simulation purpose.
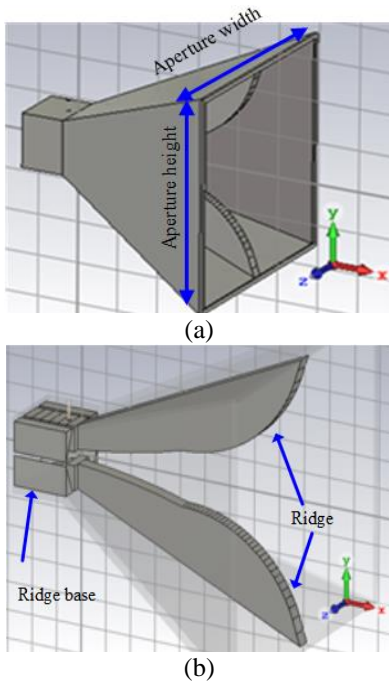

(a)

(b)

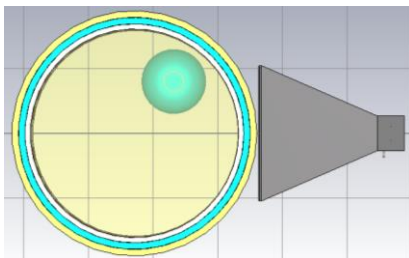Fig. 3. (a) Geometry of the proposed DRHA, and (b) illustration of adopted ridges.

Fig. 4. DRHA with head phantom model.

The simulated S_{11} and VSWR characteristics of the proposed DRHA antenna with and without head phantom model are shown in Figs. 5 and 6 respectively. It is evident from the figures that S_{11} (<10 dB) is achieved for frequency band of 0.48 GHz to 1.24 GHz and the VSWR is almost below a value of two for the observed band. The resulting E-field maps by exciting the antenna with different frequency subcarriers are shown in Figs. 7 to 10. The radiation patterns corresponding to the chosen frequencies are presented in Figs. 11 to 14. In order to evaluate values of specific absorption rate SAR inside the head phantom, we compute the power loss density and then acquire the SAR maps for different frequencies as depicted in Figs. 15 to 18.
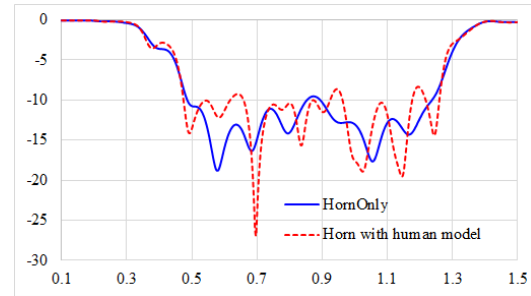

Fig. 5. Simulated S_{11} (dB) (y-axis) versus frequency (GHz) (x-axis) of the proposed antenna with and without phantom.
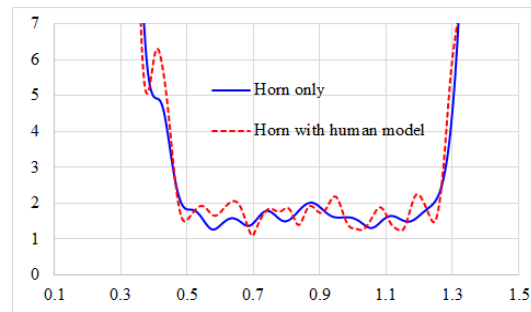

Fig. 6. Simulated VSWR (y-axis) versus frequency (GHz) (x-axis) of the proposed antenna with and without phantom.
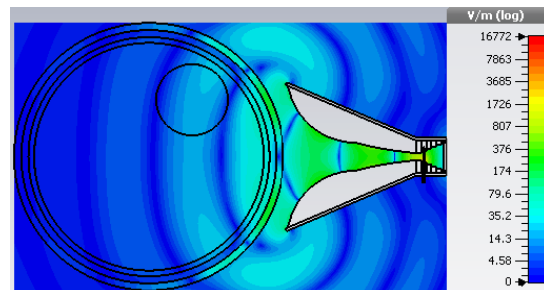

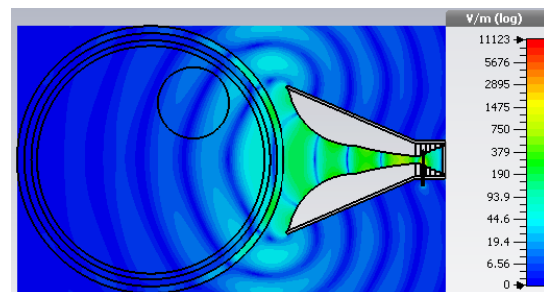Fig. 7. E-field map of the proposed DRHA antenna in the vicinity of head phantom at 0.5 GHz.

Fig. 8. E-field map of the proposed DRHA antenna in the vicinity of head phantom at 0.75 GHz.

Fig. 9. E-field map of the proposed DRHA antenna in the vicinity of head phantom at 1 GHz.

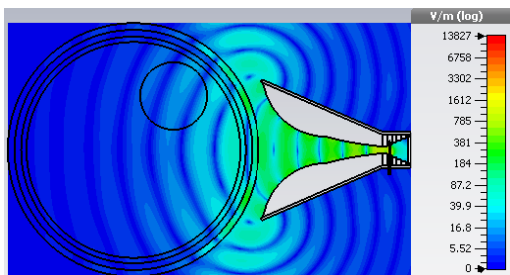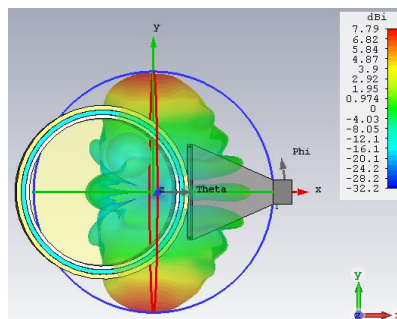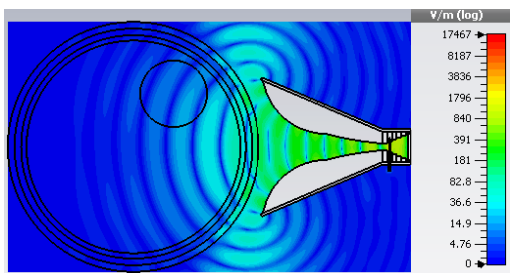Fig. 10. E-field map of the proposed DRHA antenna in the vicinity of head phantom at 1.25 GHz.

Fig. 11. Simulated radiation pattern of the proposed DRHA antenna at 0.5 GHz.

Fig. 12. Simulated radiation pattern of the proposed DRHA antenna at 0.75 GHz.
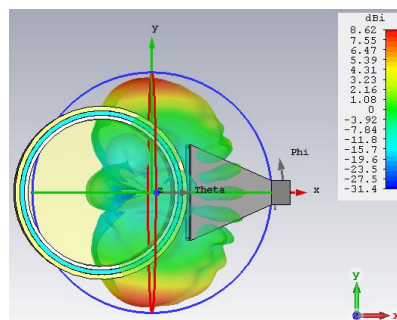

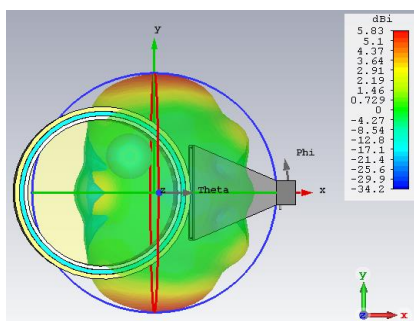Fig. 13. Simulated radiation pattern of the proposed DRHA antenna at 1 GHz.

Fig. 14. Simulated radiation pattern of the proposed DRHA antenna at 1.25 GHz.
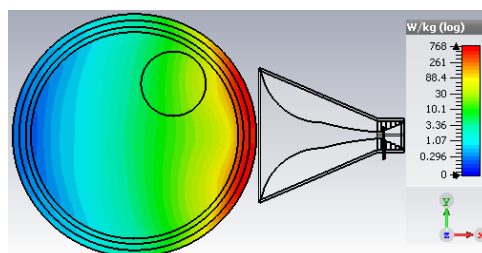

Fig. 15. Simulated SAR map inside the head phantom when the proposed DRHA antenna operates at frequecny of 0.5 GHz.
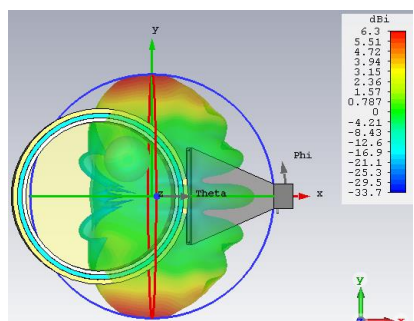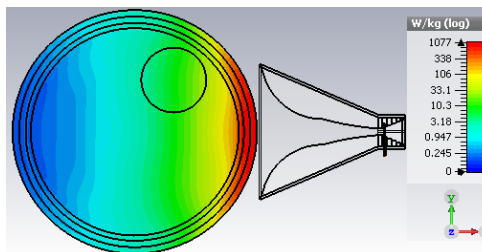

Fig. 16. Simulated SAR map inside the head phantom when the proposed DRHA antenna operates at frequecny of 0.75 GHz.
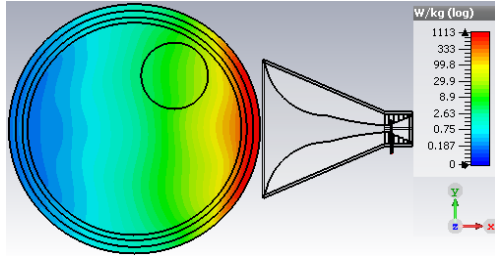
Fig. 17. Simulated SAR map inside the head phantom when the proposed DRHA antenna operates at frequecny 1 GHz.
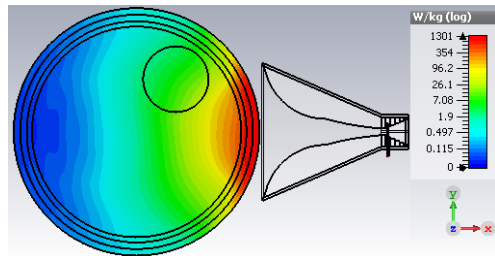

Fig. 18. Simulated SAR map inside the head phantom when the proposed DRHA antenna operates at frequecny 1.25 GHz.

As apparent from the figures, appropriate levels of SAR distribution can be achieved inside the phantom for different frequencies. However, to maximize SAR at tumor location and minimize outside the tumor, it requires wave-shaping of wideband energy radiated from an applicator array. This can be accomplished using energy localization methods such as time reversal technique.

C. Power amplifier (PA) module

The introduction of power amplifier in each channel is essential to allow deposition of enough energy into the intended tissue to raise the temperature and achieve hyperthermia therapeutic level. Wideband channels allows targeting superficial as well as deep-seated tumors. This invokes the requirement of PA providing high power levels, wideband and high efficiency characteristics. To achieve high efficiency, the PA has to be operated near its saturation, which causes the amplifier to behave non-linearly and yield harmonics and intermodulation products. This can severely degrade the performance of the energy localization. In this research, we devise a power amplifier that can exhibit high efficiency while maintaining good degree of linearity for a wideband frequency range of operation.

The recent research trend in the area of wideband power amplifier design is the use GaN HEMT field effect transistors because of its high breakdown voltage level and current density as compared to its counterpart

GaAs transistors. With the aim to achieve high power, several GaN HEMT based distributed power amplifiers are reported by researchers. It includes a wideband distributed power amplifier using a GaN HEMT to give 40.4 dBm of maximum output power with a small signal gain of 10 dB and power added efficiency (PAE) of greater than 35% when operated in 700 MHz to 4.5 GHz frequency [23]. In another research effort, an ultra-wideband GaN HEMT DA with a frequency range of 20 MHz to 3 GHz, 37 dBm output power and PAE of 27% is achieved using three GaN HEMT transistors [24]. A 5-W GaN HEMT, 0.35-8 GHz ultra-wideband power amplifier with average gain of 9 dB and PAE of 20% throughout the band is reported in [25].

In this paper we present the design of multi-octave GaN HEMT based wideband distributed power amplifier with almost flat gain of 10 dB from 0.2 GHz to 1.2 GHz. The maximum PAE achieved is 50%. This design is based on conventional distributed amplifier also known as travelling wave amplifier, consists of multiple FETs connected through drain and gate transmission lines as shown in Fig. 19.
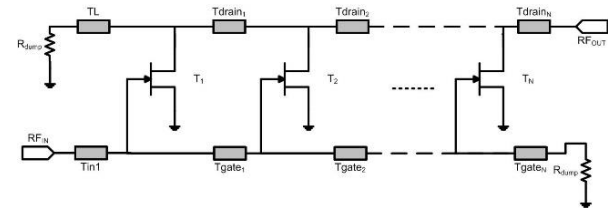

Fig. 19. Conventional distributed power amplifier.

The power is amplified at each FET and it adds up in phase with the signal at each section. Since the gain is almost the same for each amplifier, higher gain-bandwidth product can be achieved. The main disadvantage of the distributed power amplifier is its efficiency, which is typically in the range of 20-35%. The efficiency however can be increased using different techniques. One approach is to reduce losses at the gate of FET by introducing a series capacitance [26]. Another approach is based on tapering of the drain line with no termination as proposed by [27]. We included both techniques in our design.

In order to meet the output power requirement for hyperthermia treatment which typically varies between 90-110W for each channel, we choose a CREE manufactured 120 watts bare-die GaN HEMT FET (CGH60120D) [28]. A three-cell cascade topology of the distributed amplifier (DA) is adopted based on conventional design of DA and then optimized for high efficiency, gain and power. The schematic of the designed DA is shown in Fig. 20. The structure is simulated using Advance Design System (ADS) simulation software by Keysight's technologies. The values of lumped components used in the schematic are given in Table 1.
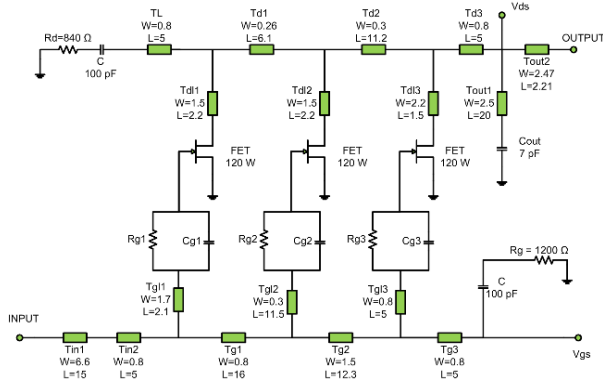
Fig. 20. Component level schematic of the proposed power amplifier.

Table 1: Lumped parameters used in schematic

Capacitors	Value (pF)	Resistors	Value (Ohms)
C	100	Rg1	710
Cout	7	Rg2	830
Cg1	0.3	Rg3	15
Cg2	5.7	Rd	840
Cg3	3	Rg	1200

The small signal simulations are carried out with the biasing conditions of Vgs = -2.5 Volts and Vds = 28 Volts. The HEMT has typically a larger gate-to-source capacitance 'Cgs' than its drain-to-source capacitance 'Cds'. In our case Cgs value is 34 pF, while, Cds is 7.7 pF at -8 Volts of Vgs as stated in the datasheet of the HEMT.

The bandwidth and efficiency can be improved by adding a series gate capacitance to lower the value of HEMT's Cgs. The simulations therefore involved two steps: firstly, without the series capacitance and secondly, with an optimized series capacitance. The values of the optimized capacitances are listed in Table 1. By adding the series capacitances to our HEMTs, their equivalent input capacitances which are directly proportional to its bandwidth can be approximated as; Ceq1 = Cgs ∥ Cg1 = 0.29 pF, Ceq2 = Cgs ∥ Cg2 = 4.88 pF, and Ceq3 = Cgs ∥ Cg3 = 2.75 pF. Thus, S_{11} and transducer power gain both are improved by adding the series gate capacitance C_{g1}, C_{g2}, and C_{g3} as illustrated in Figs. 21 and 22, respectively.

To improve output power and power added efficiency R_d and R_g are chosen to be 840 Ω, while the optimized capacitances 'C' along with drain and gate line is chosen to be 100 pF. With this configuration, maximum efficiency achieved at 1.2 GHz is 50% with maximum output power of 49 dBm as shown in Fig. 23, which corresponds to 80 watts, approximately making it suffice to be used in each channel of the proposed hyperthermia treatment system.

Fig. 21. S_{11} (dB) versus frequency (GHz), with and without series gate capacitance Cg.

Fig. 22. Transducer gian S_{21} (dB) versus frequency (GHz), with and without series gate capacitance Cg.

Fig. 23. Output power (dBm) & power added efficiency (%) versus input power (dBm) at 1.2 GHz.

D. Waveform shaping module

Energy localization in hyperthermia treatment is reported to be achieved using various techniques such as phased-arrays [29, 30], ultra-wideband beamforming approach [10], multi-frequency technique [31], transmission line approach [32, 33], time reversal techniques [34, 35],

temperature control feedback approach [36], projection algorithm [37], eigenvalue analysis [38] and SAR optimization techniques reported in [39-42].

We chose time reversal (TR) optimization technique to achieve energy localization at tumor region. As compared to other SAR or temperature optimization techniques, it is more robust, as it estimates the phases and magnitudes of E-fields directly from wave simulation rather than measured data [35]. It also allows the use of sinusoidal or pulse form of input excitation signals. Typically, TR operation involves two steps [43, 44]. In the 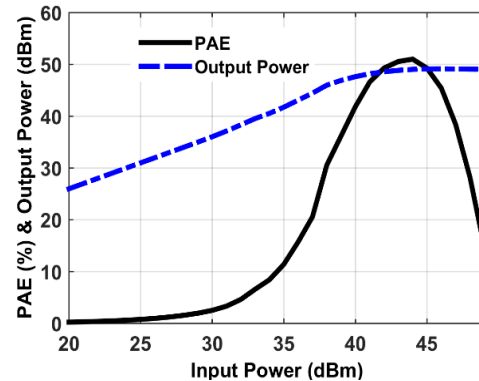first step, a virtual excitation source is placed at desired focusing position and energy is allowed to propagate through the heterogeneous head model. These field values are recorded at model surface and are processed in a time-reversed order, corresponding to conjugation in frequency domain. In the second step, the virtual source is removed and antenna applicators are placed at points of maximum field and are driven by the time-reversed signals. Because of the time invariance characteristics of EM field, the back-propagated time-reversed fields has the capability to refocus at the initial position of the virtual source. Here in this study, we use a plane of virtual source at tumor center. This plane has a dimension of 1cm x 1cm and can be considered as grid of point sources, excited by each of the subcarriers.

Mathematically, the field measured by an applicator at the phantom surface from the mth excitation point is given by:

$$f(t) = \sum_{m=1}^{M} h_m(t) \otimes e_m(t), \qquad (2)$$

or

$$f(t) = \int_{-\infty}^{+\infty} \sum_{m=1}^{M} h_m(t) e_m(t - \tau) d\tau, \qquad (3)$$

Where $\otimes$ represents the temporal convolution and $h_m(t)$ is the linear propagation operator defined by Green's function. This term includes the propagation effects of the medium from the mth excitation point to applicator. $e_m(t)$ corresponds to excitation signal of point source and $f(t)$ is the signal measured by the applicator. In frequency domain, Equation (3) can be written in matrix form as:

$$F(\omega) = H_m(\omega) E_m(\omega). \qquad (4)$$

The matrix $H_m(\omega)$ is the Fourier transform of the Green's function. By assuming spatial reciprocity condition, the propagation between applicator and virtual point sources can be represented as:

$$E_m(\omega) = H_m^T(\omega) F(\omega). \qquad (5)$$

Here H_m^T is the transpose of H_m. For the time reversal step, the time reversal operation of Green's function $[h_m(-t)]$ in time domain is equivalent to complex conjugate in frequency domain. Therefore, the time reversing the spectrum of applicator's output yields:

$$F^*(\omega) = H_m^*(\omega) E_m^*(\omega) = H_m^*(\omega) E_m(\omega). \qquad (6)$$

Here E_m is real and '*' represents the complex conjugate. By combing the previous two equations, the back-propagated signal at the initial source location can be achieved as:

$$E_{TR}(\omega) = H_m^T(\omega) F^*(\omega), \qquad (7)$$

or

$$E_{TR}(\omega) = H_m^T(\omega) H_m^*(\omega) E_m(\omega). \qquad (8)$$

Where $H_m^T(\omega) H_m^*(\omega)$ is known as time reversal (TR) operator. In this research, a time reversal (TR) tool is developed using MATLAB [45], which has the capability to interface with CST simulating environment to automate the process of field acquisition, TR processing and feeding back to the applicators.

We investigate step 2 of the TR method by considering three planes xmax, ymax and zmin located on phantom surface at maximum value of x, maximum value of y and minimum value of z positions, respectively. The field resulted by excitation of the source at tumor center are collected at these planes, and TR tool is invoked to acquire field values, calculate the conjugate, and feed it back at planes positions. The fields are then ready to be back propagated towards tumor center, which is step 2 of the TR technique. In order to visualize energy localization at tumor region, we made three cut planes at tumor center located parallel to yz, xz and xy planes. The results are shown in Figs. 24 to 27, respectively.

Figure 24 demonstrates that energy localization is more prominent in the tumor yz plane when xmax plane is chosen for step 2 of TR. When ymax plane is chosen, good energy localization is achieved in tumor xz plane as shown in Fig. 25. The focus of energy localization shifts to tumor xy plane when zmin is chosen as excitation plane for step 2 of TR. This is illustrated in Fig. 26.
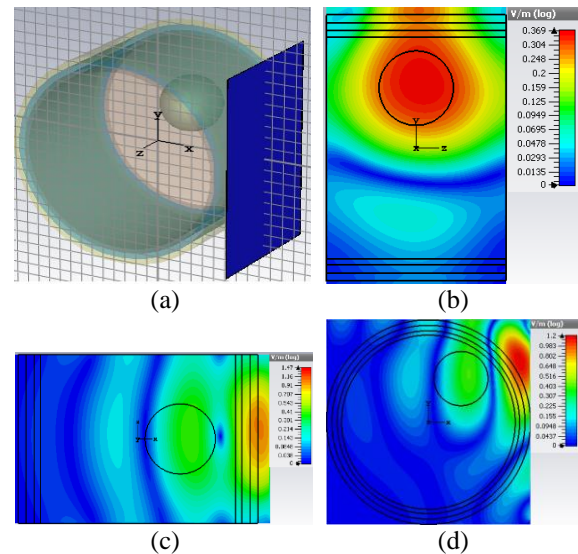

(a)   (b)

(c)   (d)

Fig. 24. Step 2 of TR energy locaization when (a) field from xmax plane is back-propagated towards tumor. Energy localization is shown at tumor center in yz (b), xz (c), and xy (d) planes.

(a)   (b)

(c)   (d)

Fig. 25. Step 2 of TR energy locaization when (a) field from ymax plane is back propogated towards tumor. Energy localization is shown at tumor center in yz (b), xz (c), and xy (d) planes.

(a)   (b)

(c)   (d)

Fig. 26. Step 2 of TR energy locaization when (a) field from zmin plane is back propogated towards tumor. Energy localization is shown at tumor center in yz (b), xz (c), and xy (d) planes.
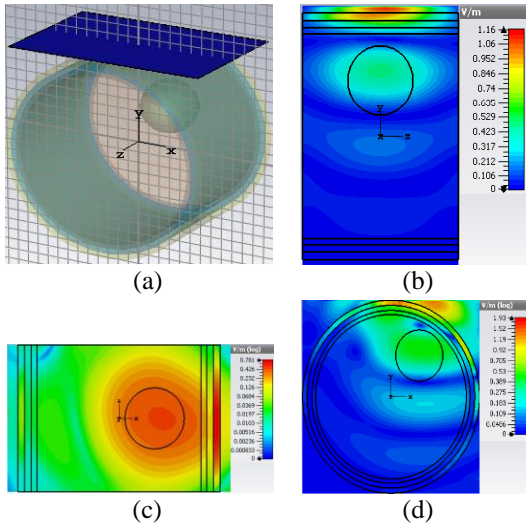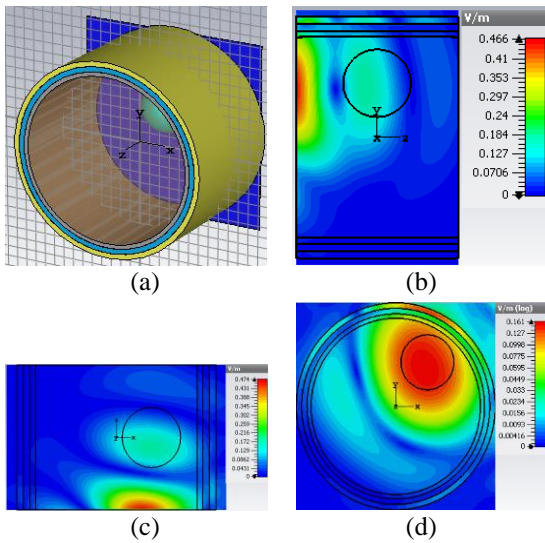
For the case when all fields at phantom surface is propagated backward to phantom in time reversal mode, the results are shown in Fig. 27. We now extend the results achieved in Fig. 27 to 3D visualization by considering two cases: narrowband and wideband excitation and investigating the results of TR energy localization for both cases. The results achieved for narrowband case is shown in Fig. 28, when all the four planes at phantom surface are excited with a single frequency carrier of 0.5, 0.75, 1 and 1.25 GHz respectively.

The figure reveals the fact that good penetration of EM signal is achieved for low frequencies while sharp focus is accomplished for high frequencies. It implies that adopting a wideband TR approach can deliver enhanced localization of energy. Results for the wideband TR energy localization are shown in Figs. 29 and 30.

For wideband operation, the results demonstrate the fact that increasing the number of frequency subcarriers can further improve energy localization. Heat generated, because of hotspots at the head interface, can be cooled down by the water coupling medium present between the applicator and the head.

(a)   (b)

(c)   (d)
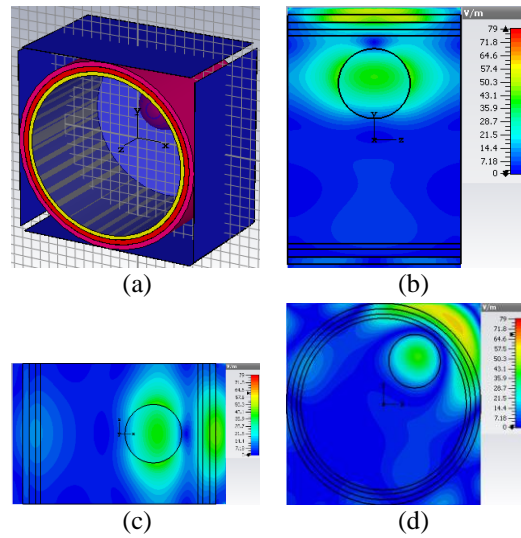
Fig. 27. Step 2 of TR energy locaization when (a) fields from four planes are back propogated towards tumor. Energy localization is shown at tumor center in yz (b), xz (c), and xy (d) planes.

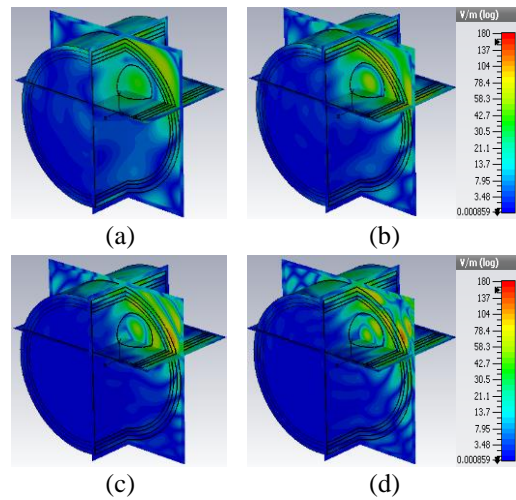(a)   (b)

(c)   (d)

Fig. 28. 3D view of energy localization at tumor center for narrowband TR case when frequency is (a) 0.5 GHz, (b) 0.75 GHz, (c) 1 GHz, and (d) 1.25 GHz.
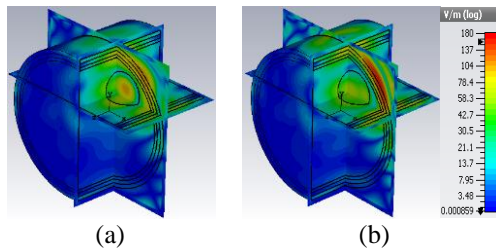
Fig. 29. 3D view of energy localization at tumor center for wideband TR case when (a) two frequency subcarriers 0.5 and 0.75 GHz are combined, and (b) three frequency subcarriers 0.5, 0.75, and 1 GHz are combined.
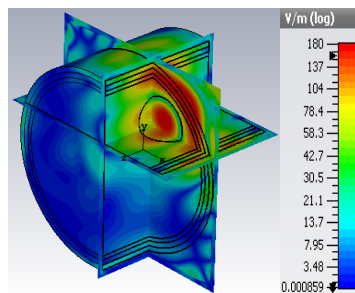

Fig. 30. 3D view of energy localization at tumor center for wideband TR case when four frequency subcarriers 0.5, 0.75, 1.0 and 1.25 GHz are combined.

IV. DISCUSSION AND CONCLUSIONS

A wideband, hyperthermia treatment system with the potential of enhancing energy localization is investigated and presented. The incorporated multi-channel configuration allows enhancement in energy focus. The proposed system is described in big data domain with the aim to identify system parameters to expedite energy accumulation process with precision and accuracy. A modular description of the proposed system is presented focusing on the functionality of each module under wideband excitation. With the adopted modular approach, the system provides an increase in the number of degrees of freedom to allow performance improvement. A robust wideband waveform shaping technique is proposed based on an optimization tool to maximize SAR values at the affected regions and minimize the values in healthy tissues. The achieved results show that wideband energy can be controlled to target deep-seated tumor effectively.

Clinical adaptation of such systems requires the development of real time optimization tool, which can be achieved using hardware acceleration and cluster computing techniques. Robust real time temperature monitoring is needed to provide a feedback mechanism to control energy excitation. With addressing of clinical challenges, the proposed system can improve the efficacy of hyperthermia treatment and enhance patient comfort and safety.

REFERENCES

[1] A. Shitzer and R. C. Eberhart, *Heat Transfer in Medicine and Biology: Analysis and Applications*. vol. 1, Plenum Press, 1985.

[2] H. Trefna and M. Persson, "Heating of deep seated tumours using microwaves radiation," in *ACES*, Verona, Italy, 2007.

[3] X. Wu, B. Liu, and B. Xu, "Theoretical evaluation of high frequency microwave ablation applied in cancer therapy," *Applied Thermal Engineering*, vol. 107, pp. 501-507, 2016.

[4] J. Mallorqui, A. Broquetas, L. Jofre, and A. Cardama, "Non-invasive active thermometry with a microwave tomographic scanner in hyperthermia treatments," *Applied Computational Electromagnetics Society (ACES) Journal*, vol. 7, pp. 121-127, 1992.

[5] M. M. Paulides, P. R. Stauffer, E. Neufeld, P. F. Maccarini, A. Kyriakou, R. A. Canters, C. J. Diederich, J. F. Bakker, and G. C. Van Rhoon, "Simulation techniques in hyperthermia treatment planning," *International Journal of Hyperthermia*, vol. 29, pp. 346-357, 2013.

[6] S. Fodeh and Q. Zeng, "Mining big data in biomedicine and health care," *Journal of Biomedical Informatics*, vol. 63, p. 400, 2016.

[7] K. J. Archer, K. Dobbin, S. Biswas, R. S. Day, D. C. Wheeler, and H. Wu, "Computer simulation, bioinformatics, and statistical analysis of cancer data and processes," *Cancer Informatics*, vol. 14, p. 247, 2015.

[8] J. Roski, G. W. Bo-Linn, and T. A. Andrews, "Creating value in health care through big data: Opportunities and policy implications," *Health Affairs*, vol. 33, pp. 1115-1122, 2014.

[9] P. Groves, B. Kayyali, D. Knott, and S. V. Kuiken, "*The 'big data' revolution in healthcare: Accelerating value and innovation*," Center for US Health System Reform, McKinsey & Company, 2013.

[10] M. Converse, E. J. Bond, B. Veen, and S. C. Hagness, "A computational study of ultra-wideband versus narrowband microwave hyperthermia for breast cancer treatment," *IEEE Transactions on Microwave Theory and Techniques*, vol. 54, pp. 2169-2180, 2006.

[11] M. N. Tabassum, I. Elshafiey, and M. Alam, "Enhanced noninvasive imaging system for dispersive highly coherent space," in *IEEE International Conference on Acoustics, Speech and Signal Processing (ICASSP)*, pp. 912-916, 2015.

[12] M. N. Tabassum, I. Elshafiey, and M. Alam, "Efficient techniques to enhance nearfield imaging of human head for anomaly detection," in *IEEE International Symposium Medical Measurements and Applications (MeMeA)*, pp. 565-569, 2015.

[13] M. N. Tabassum, I. Elshafiey, and M. Alam, "Compressed sensing based nearfield electromagnetic imaging," in *IEEE International Conference on Control System, Computing and Engineering (ICCSCE)*, pp. 571-575, 2014.

[14] M. Aldhaeebi and I. Elshafiey, "New antenna design for hyperthermia treatment of human head," in *IEEE 16th International Conference on Computer Modelling and Simulation, UKSim-AMSS*, 2014, pp. 96-100.

[15] A. Alkhaibari, A. F. Sheta, and I. Elshafiey, "Notched anti-podal Vivaldi antenna for biomedical applications," in *IEEE 7th International Conference on Modeling, Simulation, and Applied Optimization (ICMSAO)*, pp. 1-4, 2017.

[16] M. M. M. Ali, O. Haraz, I. Elshafiey, S. Alshebeili, and A.-R. Sebak, "Efficient single-band and dual-band antennas for microwave imaging and hyperthermia treatment of brain tumors," in *IEEE International Conference on Control System, Computing and Engineering (ICCSCE)*, pp. 597-600, 2014.

[17] G. Chakaravarthi and K. Arunachalam, "Design and characterisation of miniaturised cavity-backed patch antenna for microwave hyperthermia," *International Journal of Hyperthermia*, vol. 31, pp. 737-748, Mar. 10, 2015.

[18] S. Singh and S. P. Singh, "Theoretical and simulation studies on water-loaded metal diagonal horn antenna for hyperthermia application," *Progress In Electromagnetics Research C*, vol. 58, pp. 105-115, 2015.

[19] A. Mallahzadeh and A. Imani, "Modified double-ridged antenna for 2-18 GHz," *Applied Computational Electromagnetics Society (ACES) Journal*, vol. 25, p. 137, 2010.

[20] Q. Yang, X. Zhao, and Y. Zhang, "Electromagnetic analysis on propagation characteristics of CRLH waveguide loaded with double ridge corrugations," *Progress In Electromagnetics Research C*, vol. 75, pp. 1-11, 2017.

[21] M. Botello-Perez, H. Jardon-Aguilar, and I. G. Ruíz, "Design and simulation of a 1 to 14 GHz broadband electromagnetic compatibility DRGH antenna," in I*EEE 2nd International Conference on Electrical and Electronics Engineering*, pp. 118-121, 2005.

[22] S. I. Latif, D. Flores-Tapia, S. Pistorius, and L. Shafai, "Design and performance analysis of the miniaturised water-filled double-ridged horn antenna for active microwave imaging applications,"

[23] H. Y. Amin and B. Yarman, "Distributed wideband power amplifier using reactive coupled line feedback structure," in *IEEE 2nd International Conference on Knowledge-Based Engineering and Innovation (KBEI)*, pp. 91-94, 2015.

[24] S. Lin, M. Eron, and A. E. Fathy, "Development of ultra wideband, high efficiency, distributed power amplifiers using discrete GaN HEMTs," *IET Circuits, Devices & Systems*, vol. 3, pp. 135-142, 2009.

[25] A. Sayed, A. A. Tanany, and G. Boeck, "5W, 0.35-8 GHz linear power amplifier using GaN HEMT," in *European Microwave Conference (EuMC)*, pp. 488-491, 2009.

[26] Y. Ayasli, J. Vorhaus, R. Mozzi, and L. Reynolds, "Monolithic GaAs travelling-wave amplifier," *Electronics Letters*, vol. 17, p. 413, 1981.

[27] E. L. Ginzton, W. R. Hewlett, J. H. Jasberg, and J. D. Noe, "Distributed amplification," *Proceedings of the IRE*, vol. 36, pp. 956-969, 1948.

[28] Wolfspeed A Cree Company. 120 Watts RF GaN HEMT (CGH60120D). Available: http://www. wolfspeed. com/cgh60120d

[29] A. J. Fenn, V. Sathiaseelan, G. A. King, and P. R. Stauffer, "Improved localization of energy deposition in adaptive phased-array hyperthermia treatment of cancer," *Lincoln Laboratory Journa*l, vol. 9, 1996.

[30] C. M. Furse, "A survey of phased arrays for medical applications," *Applied Computational Electromagnetics Society (ACES) Journal*, vol. 21, pp. 365-379, 2006.

[31] S. Jacobsen and F. Melandsø, "The concept of using multifrequency energy transmission to reduce hot spots during deep-body hyperthermia," *Annals of Biomedical Engineering*, vol. 30, pp. 34-43, 2002.

[32] N. Nizam-Uddin and I. Elshafiey, "Transmission line approach for energy localization in wideband hyperthermia treatment system," in *IEEE 5th International Conference on Electronic Devices, Systems and Applications (ICEDSA)*, pp. 1-4, 2016.

[33] N. Nizam-Uddin and I. Elshafiey, "Enhanced energy localization with wideband hyperthermia treatment system," *Applied Computational Electromagnetics Society Journal*, vol. 32, pp. 389-396, 2017.

[34] P. Takook, H. D. Trefná, A. Fhager, and M. Persson, "Evaluation of the 3D time reversal method for hyperthermia treatment planning in head and neck tumors," in *9th European Conference on Antennas and Propagation (EuCAP)*, pp. 1-5, 2015.

[35] H. D. Trefná, J. Vrba, and M. Persson, "Time-

IET Microwaves, Antennas & Propagation, vol. 9, pp. 1173-1178, 2015.

reversal focusing in microwave hyperthermia for deep-seated tumors," *Physics in Medicine and Biology*, vol. 55, p. 2167, 2010.

[36] F. Bardati, A. Borrani, A. Gerardino, and G. A. Lovisolo, "SAR optimization in a phased array radiofrequency hyperthermia system," *IEEE Transactions on Biomedical Engineering*, vol. 42, pp. 1201-1207, 1995.

[37] C. A. Liontas and P. Knott, "An alternating projections algorithm for optimizing electromagnetic fields in regional hyperthermia," in *IEEE 10th European Conference on Antennas and Propagation (EuCAP)*, pp. 1-5, 2016.

[38] R. M. C. Mestrom, J. P. van Engelen, M. C. van Beurden, M. M. Paulides, W. C. M. Numan, and A. G. Tijhuis, "A refined eigenvalue-based optimization technique for hyperthermia treatment planning," in *IEEE 8th European Conference on Antennas and Propagation (EuCAP)*, pp. 2010-2013, 2014.

[39] M. Aldhaeebi, M. Alzabidi, and I. Elshafiey, "Genetic algorithm optimization of SAR distribution in hyperthermia treatment of human head," in *IEEE 1st International Conference on Artificial Intelligence, Modelling and Simulation (AIMS)*, pp. 92-97, 2013.

[40] M. Aldhaeebi, M. Alzabidi, and I. Elshafiey, "Optimization of UWB antenna array for hyperthermia treatment of brain tumor," in *IEEE Saudi International Electronics, Communications and Photonics Conference (SIECPC)*, pp. 1-6, 2013.

[41] P. T. Nguyen, A. Abbosh, and S. Crozier, "Three-dimensional microwave hyperthermia for breast cancer treatment in a realistic environment using particle wwarm optimization," *IEEE Transactions on Biomedical Engineering*, 2016.

[42] N. Nizam-Uddin and I. Elshafiey, "Enhanced energy localization in hyperthermia treatment based on hybrid electromagnetic and ultrasonic system: Proof of concept with numerical simulations," *BioMed Research International*, vol. 2017, p. 18, 2017.

[43] R. Carminati, R. Pierrat, J. De Rosny, and M. Fink, "Theory of the time reversal cavity for electromagnetic fields," *Optics Letters*, vol. 32, pp. 3107-3109, 2007.

[44] D. Cassereau and M. Fink, "Time-reversal of ultrasonic fields. III. Theory of the closed time-reversal cavity," *IEEE Transactions on Ultrasonics, Ferroelectrics, and Frequency Control*, vol. 39, pp. 579-592, 1992.

[45] MathWorks. MATLAB: The Language of Technical Computing. Available: http://www.mathworks.com/

N. Nizam-Uddin received his B.S. degree in Electrical Engineering from NWFP University of Engineering & Technology Peshawar, Pakistan in 2002 and M.S. from Edinburgh Napier University, UK in 2005, majoring Communication. He is currently pursuing Ph.D. in Electrical Engineering at King Saud University. His research interest includes antenna theory, bio-electromagnetics, biomedical physics and microwave engineering.

Wazie M. Abdulkawi is currently pursuing Ph.D. at Electrical Engineering Department in King Saud University. He received M.S. in Electrical Engineering from King Saud University in 2013 and B.Sc. in Communication Engineering from Ibb University, Ibb, Yemen in 2007. His research interest includes antenna theory, RFID design, electromagnetics and microwave engineering.

Waqar Ahmad Malik received his B.S. degree in Electrical Engineering from NWFP University of Engineering & Technology Peshawar, Pakistan in 2004 and M.S. from The University of Hull, UK in 2006, majoring Radio Systems Engineering. He is currently pursuing Ph.D. in Electrical Engineering at King Saud University. His research interest includes optimization of microwave circuits, broadband matching circuits, and microwave amplifiers design.

Ibrahim Elshafiey received his B.S. degree in Communications and Electronics Engineering from Cairo University in 1985. He obtained his M.S. and Ph.D. degrees from Iowa State University in 1992 and 1994 respectively. He is currently a Professor in the Electrical Engineering Department at King Saud University. His research interests include computational electromagnetics, biomedical imaging, communication systems and non-destructive evaluation.

Abdel Fattah Sheta graduated from the Faculty of Engineering, Alexandria University, Egypt in 1985. He received the M.Sc. degree in Electrical Engineering from Cairo University, Egypt, in 1991. In 1996, he received the Ph.D. degree in Microwave Circuits Analysis and Design from ENST, Université de Bretagne Occidentale, France. He is a Full Professor at Electrical Engineering Department at King Saud University. His current research interests include reconfigurable RF system, UWB systems, microstrip antennas, antennas for hyperthermia applications, microstrip filters, planar and uniplanar MIC's and MMIC's, and power amplifiers.